Towards the prediction of the Mars 2020 heatshield material response

Jeremie B.E. Meurisse[2], Joshua D. Monk[3], Arnaud Borner[2], Joseph Ferguson[2], Francesco Panerai[3] & Nagi N. Mansour[1]
[1]NASA Ames Research Center [2] Science and Technology Corporation at NASA Ames Research Center [3]AMA Inc. at NASA Ames Research Center

AW-2018, September
University of Vermont

Introduction

NASA's next mission to Mars, the **Mars 2020**, will use the same heatshield of the Mars Science Laboratory (**MSL**) for thermal protection during entry, descent and landing. The heatshield is a tiled system made of Phenolic Impregnated Carbon Ablators (**PICA**) blocks [1]. PICA is a lightweight carbon fiber/polymeric resin material that offers excellent performances for protecting probes during planetary entry. The Mars Entry Descent and Landing Instrument (**MEDLI**) suite on MSL offers unique in-flight validation data for models of atmospheric entry and material response. MEDLI recorded, among others, time-resolved in-depth temperature data of PICA using thermocouple sensors assembled in the MEDLI Integrated Sensor Plugs (**MISP**). The objective of this work is to compare the thermal response of the MSL heatshield to the MISP **flight data**. In preparation to Mars 2020 post-flight analysis, the predictive material response capability is benchmarked against MEDLI flight data.

Porous material Analysis Toolbox based on OpenFOAM (PATO)

The computational model is a generic mass and heat transfer model for porous reactive materials containing several solid phases and a single gas phase. The detailed chemical interactions occurring between the solid phases and the gas phase are modeled at the pore scale assuming Local Thermal Equilibrium (**LTE**). This model is implemented in the Porous material Analysis Toolbox based on OpenFOAM (**PATO**) [2,3,4], a C++ top level module of the open source computational fluid dynamics software program **OpenFOAM**. The present work compares PATO simulations to MISP flight data using the shallowest thermocouple as thermal boundary conditions (**TC1 driver**) or the aerothermal environment boundary conditions including radiation (**environment BC** in Fig. 2-3) at different MISP locations. The PATO material response model, used in Fig. 4-9, includes the elemental mass conservation and the equilibrium chemistry using the composition of the elements.

Prediction methodology

Figure 1 shows the different tools used for the MSL material response. The aerothermal environment at various Knudsen regimes is fed to **PATO** as surface boundary conditions. In the rarified regime, the environment around the MSL aeroshell is computed using the Direct Simulation Monte Carlo code **SPARTA** [5], while in the continuum regime the CFD code Data Parallel Line Relaxation (**DPLR**) [6] is used. The radiation heating from the environment is added to the surface energy balance by computing radiative flux at Mars entry conditions using the Nonequilibrium air radiation (**NEQAIR**) program [7]. Effective material properties for PICA are obtained through a combination of experiments and predictive simulation using the Porous Microstructure Analysis (**PuMA**) software [8]. The pyrolysis reactions are calibrated using experimental data [11] and **Dakota**. The open source third party library **Mutation++**, produced by the von Karman Institute for Fluid Dynamics, is dynamically linked to compute equilibrium chemistry compositions and thermodynamic and transport properties [9].

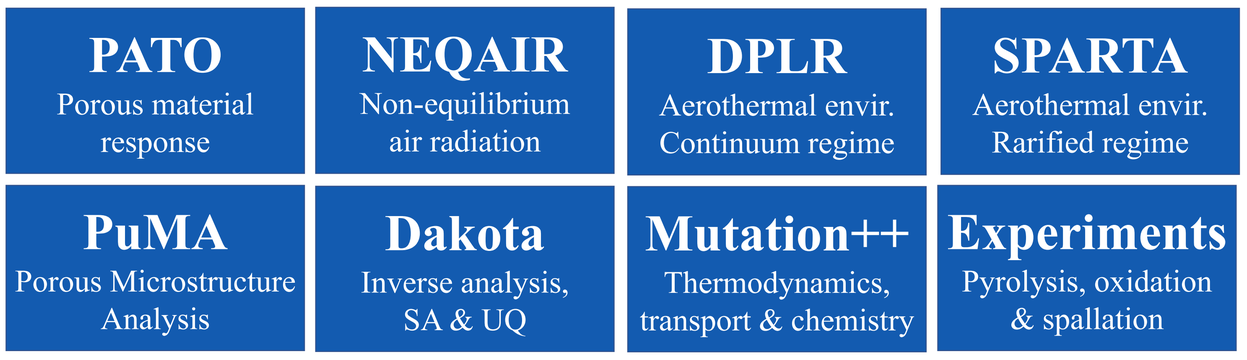

Fig. 1 Tool collections for material response prediction of thermal protection systems

Environment Boundary Conditions

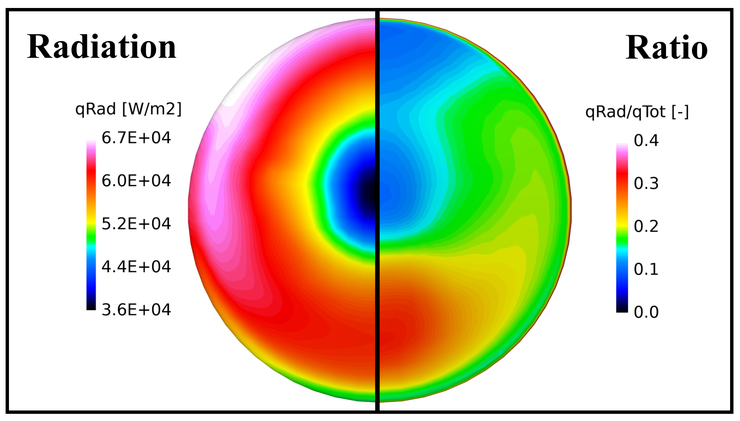

Fig. 2 Radiative heat flux at the heatshield front surface (75 s)

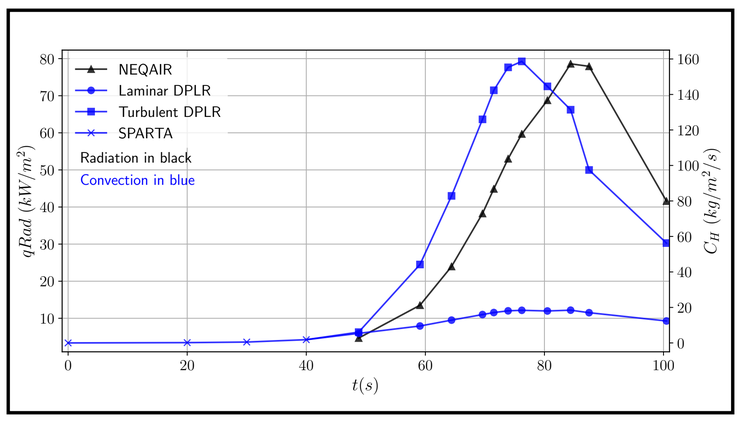

Fig. 3 Radiative and convective inputs over time at MISP2

PATO simulation vs MISP flight data: Elemental conservation + equilibrium chemistry

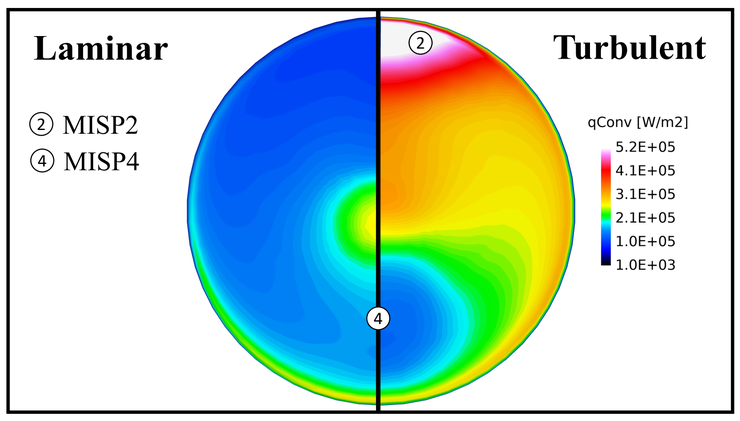

Fig. 4 Convective heat flux at the heatshield front surface (75 s)

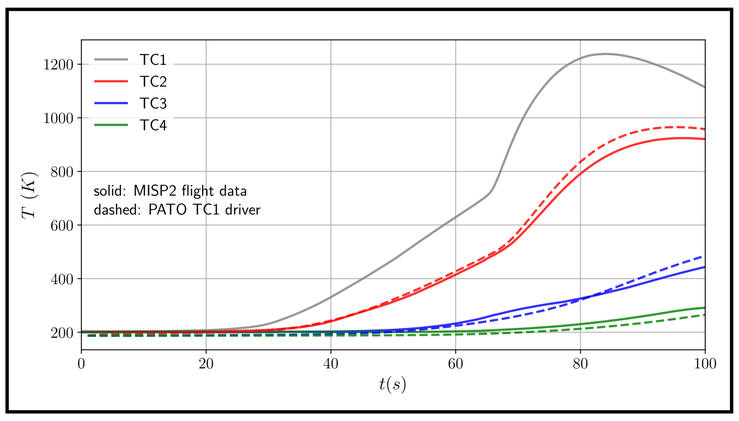

Fig. 5 PATO response using TC1 driver compared to MISP2

Fig. 6 PATO response using the environment BC compared to MISP2

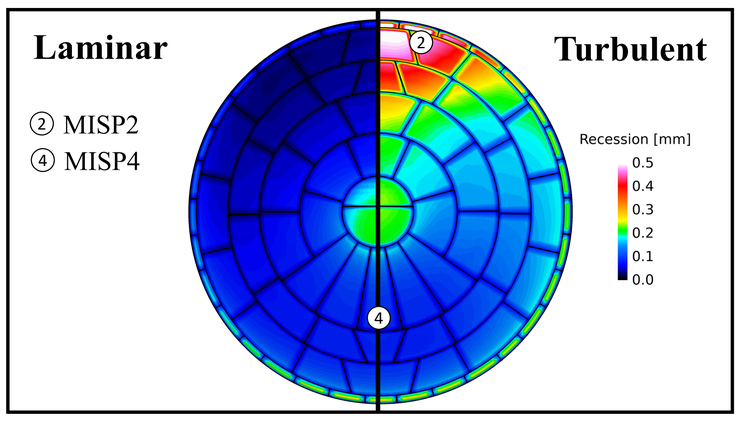

Fig. 7 Recession solution at the heatshield front surface (75 s)

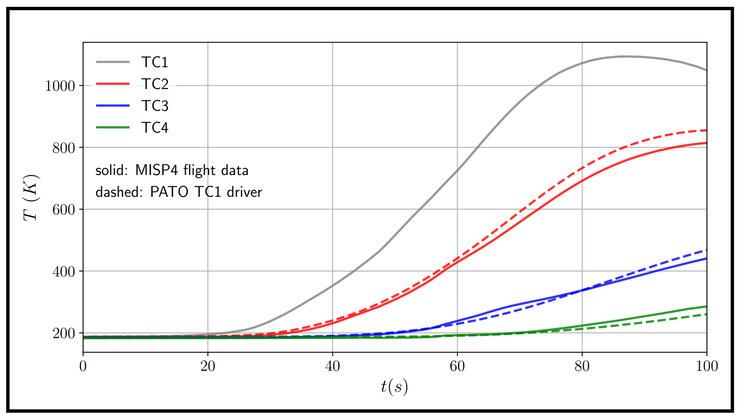

Fig. 8 PATO response using TC1 driver compared to MISP4

Fig. 9 PATO response using the environment compared to MISP4

- Mars non-equilibrium chemistry with 8 species in SPARTA, DPLR and NEQAIR
- 3D mapping method from Tecplot files using local Galerkin projection [4]
- Radiation analysis was run on all 11 CFD trajectory points at 202 radial points on the half-body heatshield solutions. 172 points used tangential slab method and 30 points used full angular integration methods in NEQAIR [7]
- 4 trajectory points in SPARTA [5] which uses Variable Soft Sphere (VSS) model with high temperature transport calibration [5]
- 11 trajectory points in DPLR which uses a laminar or a Menter Shear Stress Transport (SST) turbulence model [6]
- Radiative heat flux is up to 35% of the total heat flux at the heating peak (75 s)

- PICAv3.3 material properties [10] V&V by FIAT, TITAN and experimental arc jet data
- Porosity and permeability properties using PuMA and 3D tomography images [8]
- Elemental pyrolysis reactions calibrated by experimental data [11] using Dakota library
- PATO thermal response using TC1 driver in good agreement with MISP2 and MISP4 flight data
- MISP2 data is located between the PATO response using laminar and turbulent DPLR environment
- MISP4 data is higher at the heating peak than the PATO thermal response

References

[1] M.J. Wright et al. (2009), AIAA Paper, 2009-423.
[2] J. Lachaud et al. (2014), J Thermophys Heat Tran, 28, 191–202.
[3] J. Lachaud et al. (2017), Int J Heat Mass Tran, 108, 1406–1417.
[4] J. B.E. Meurisse et al. (2018), Aerosp Sci Technol, 76, 497-511.
[5] M. Gallis et al. (2014), AIP Conference Proceedings. Vol. 1628. No. 1.
[6] M.J. Wright et al. (2009), NASA TM–2009-215388.
[7] C. Park (1985), NASA TM-86707.
[8] J. Ferguson et al. (2018), SoftwareX 7 81-87.
[9] J. B. Scoggins et al. (2014), AIAA Paper, 2014-2966.
[10] F. Milos (2007).
[11] B. Bessire (2014), ACS applied materials & interfaces 7.3.